DOI: 10.1021/ic100361y

Inorganic Chemistry
Article

Synthesis, Structure, and Characterization of the Series $BaBi_{1-x}Ta_xO_3$ ($0 \leq x \leq 0.5$)

Hui Wang,[‡] Chun-Hai Wang,[§] Guobao Li,*[,†] Tounan Jin,*[,‡] Fuhui Liao,[†] and Jianhua Lin*[,†]

[†]*Beijing National Laboratory for Molecular Sciences, State Key Laboratory of Rare Earth Materials Chemistry and Applications, College of Chemistry and Molecular Engineering, Peking University, Beijing 100871, People's Republic of China,* [‡]*College of Material Science and Engineering, Beijing University of Technology, Beijing 100022, People's Republic of China, and* [§]*School of Physics, Peking University, Beijing 100871, People's Republic of China*

Received February 22, 2010

The series $BaBi_{1-x}Ta_xO_3$ ($0 \leq x \leq 0.5$) has been synthesized by traditional solid-state reactions. Their structures are analyzed by the combinational use of X-ray, neutron, and converged-beam electron diffractions. They all crystallize in *P*1. FTIR and Raman data confirm that an inversion center is absent in the crystal structure of the series $BaBi_{1-x}Ta_xO_3$ ($0 \leq x \leq 0.5$). No obvious P-E (polarization-electrical field) loops are observed for them.

Introduction

The discovery of superconductivity in doped $BaBiO_3$ has induced much research on $BaBiO_3$.[1−6] $BaBiO_3$ is reported to contain both Bi^{3+} and Bi^{5+} with a rock salt-like ordering in a perovskite-type framework[7−10] and crystallizes in $I2/m$ below 152 °C,[7−14] in $R\bar{3}$ between 152 and 620 °C,[7,9,10,14] and in $Fm\bar{3}m$ above 620 °C.[14] Bi in $BaBiO_3$ can be replaced by many elements.[15−20] For example, $BaBi_{0.5}M_{0.5}O_3$ (M = Sb, Ta, or Yb) is reported to be rhombohedral in $R\bar{3}$ at room temperature,[15−18] which is isostructural to $BaBiO_3$ between 152 and 620 °C. Therefore, one may expect that phase transitions in the system $BaBi_{1-x}M_xO_3$ ($0 \leq x \leq 0.5$, M = Sb, Ta, or Yb) can be induced by composition besides temperature as reported in many other systems:[21−23] at least two solid solutions related to $BaBiO_3$ (phase I, $I2/m$) and $BaBi_{0.5}M_{0.5}O_3$ (phase II, $R\bar{3}$) and one two-phase region (phase I + phase II) will be observed (if new phases appear, more than one two-phase region should be observed).

There are also several reports suggesting that $BaBiO_3$ does not crystallize in $I2/m$ below 152 °C. Sugai has suggested that an inversion center is absent in the crystal structure of $BaBiO_3$ from Raman and infrared reflection spectra of a single crystalline specimen at low temperature.[24] Hashimoto has further suggested that the space group of $BaBiO_3$ is *P*1 at

*To whom correspondence should be addressed. E-mail: liguobao@pku.edu.cn; tnjinkim@bjut.edu.cn; jhlin@pku.edu.cn. Tel: (8610)62750342. Fax: (8610)62753541.

(1) Cava, R. J.; Batlogg, B.; Krajewski, J. J.; Farrow, R.; Rupp, L. W.; White, A. E.; Short, K.; Peck, W. F.; Kometani, T. *Nature* **1988**, *332*, 814.
(2) Kumar, P. *Phys. Rev. B* **2003**, *68*, 064505.
(3) Inumaru, K.; Miyata, H.; Yamanaka, S. *Phys. Rev. B* **2008**, *78*, 132507.
(4) Hase, I.; Yanagisawa, T. *Phys. Rev. B* **2007**, *76*, 174103.
(5) Hashimoto, T.; Yamaguchi, M.; Sakurai, Y.; Oikawa, E. *J. Phys. Chem. Solids* **2008**, *69*, 284.
(6) Franchini, C.; Kresse, G.; Podloucky, R. *Phys. Rev. Lett.* **2009**, *102*, 256402.
(7) Cox, D. E.; Sleight, A. W. *Solid State Commun.* **1976**, *19*, 969.
(8) Thornton, G.; Jacobson, A. J. *Acta Crystallogr. Sect. B: Struct. Commun.* **1978**, *34*, 351.
(9) Cox, D. E.; Sleight, A. W. *Acta Crystallogr. Sect. B: Struct. Commun.* **1979**, *35*, 1.
(10) Pei, S. Y.; Jorgensen, J. D.; Dabrowski, B.; Hinks, D. G.; Richards, D. R.; Mitchell, A. W.; Newsam, J. M.; Sinha, S. K.; Vaknin, D.; Jacobson, A. J. *Phys. Rev. B* **1990**, *41*, 4126.
(11) Oda, M.; Hidaka, Y.; Katsui, A.; Murakami, T. *Solid State Commun.* **1985**, *55*, 423.
(12) Koyama, Y.; Ishimaru, M. *Phys. Rev. B* **1992**, *45*, 9966.
(13) Hashimoto, T.; Hirasawa, R.; Kobayashi, T.; Hirai, H.; Tagawa, H.; Mizusaki, J.; Toraya, H.; Tanaka, M.; Ohsumi, K. *Solid State Commun.* **1997**, *102*, 561.
(14) Zhou, Q. D.; Kennedy, B. J. *Solid State Commun.* **2004**, *132*, 389.
(15) Fu, W. T. *Solid State Commun.* **2000**, *116*, 461.
(16) Zhou, Q. D.; Kennedy, B. J. *Solid State Sci.* **2005**, *7*, 287.
(17) Harrison, W. T. A.; Reis, K. P.; Jacobson, A. J.; Schneemeyer, L. F.; Waszczak, J. V. *Chem. Mater.* **1995**, *7*, 2161.
(18) Wallwork, K. S.; Kennedy, B. J.; Zhou, Q. D.; Lee, Y.; Vogt, T. *J. Solid State Chem.* **2005**, *178*, 207.
(19) Fu, W. T.; Polderman, M. J.; Mulder, F. M. *Mater. Res. Bull.* **2000**, *35*, 1205.
(20) Sleight, A. W.; Gillson, J. L.; Bierstedt, P. E. *Solid State Commun.* **1975**, *17*, 27.
(21) Li, G. B.; Uesu, Y.; Kohn, K. *J. Solid State Chem.* **2002**, *164*, 98.
(22) Li, G. B.; Kuang, X. J.; Tian, S. J.; Liao, F. H.; Jing, X. P.; Uesu, Y.; Kohn, K. *J. Solid State Chem.* **2002**, *165*, 381.
(23) Li, G. B.; You, L. P.; Wei, W. T.; Lu, Y.; Ju, J.; Wannberg, A.; Rundlof, H.; Zou, X. D.; Yang, T.; Tian, Sh. J.; Liao, F. H.; Toyota, N.; Lin, J. H. *J. Am. Chem. Soc.* **2005**, *127*, 1409.
(24) Sugai, S. *Phys. Rev. B* **1987**, *35*, 3621.

Published on Web 05/06/2010

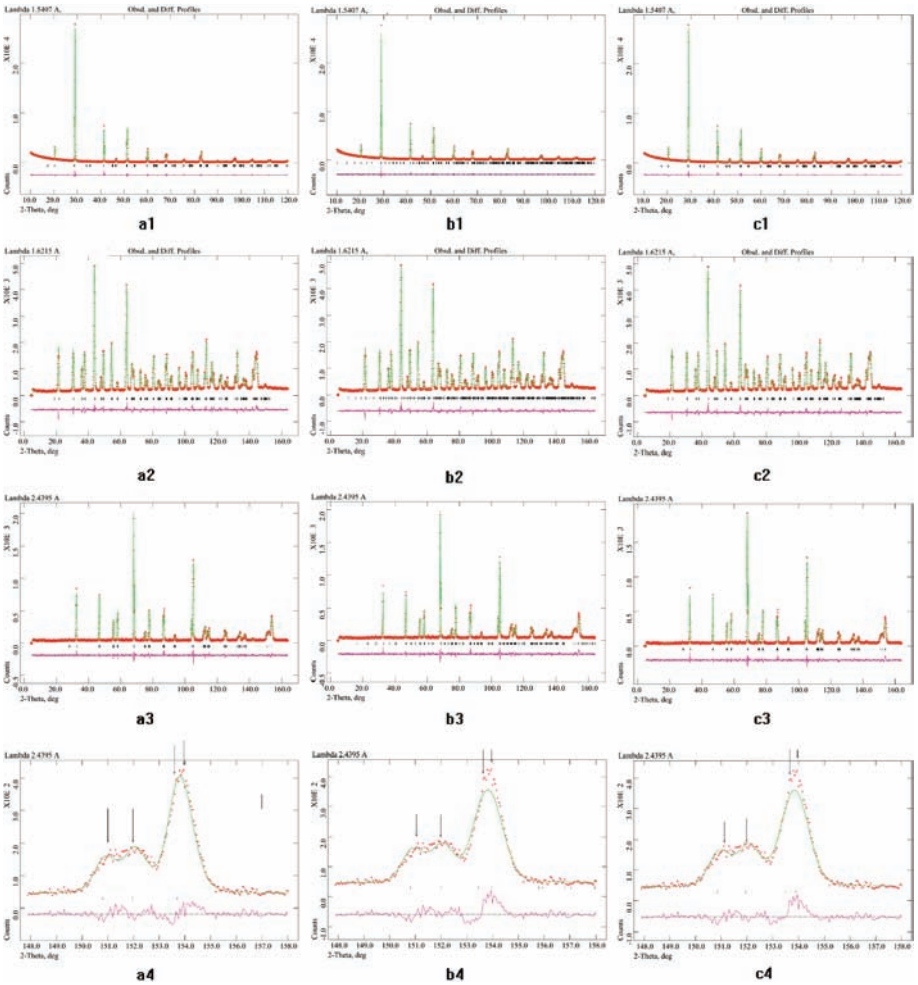

Figure 1. Rietveld plots of powder X-ray and neutron diffraction patterns for $BaBiO_3$ using different models: model 1 (a1, X-ray (λ = 0.15407 nm); a2, neutron (λ = 0.16215 nm); a3, neutron (λ = 0.24395 nm); a4, part of a3), 2 (b1, X-ray (λ = 0.15407 nm); b2 (λ = 0.16215 nm); b3, neutron (λ = 0.24395 nm); b4, part of b3), and 3 (c1, X-ray (λ = 0.15407 nm); c2 (λ = 0.16215 nm); c3, neutron (λ = 0.24395 nm); c4, part of c3). The symbol + represents the observed value, the solid line represents the calculated value; the marks below the diffraction patterns are the calculated reflection positions, and the difference curve is shown at the bottom of the figure.

room temperature by using convergent-beam electron diffraction (CBED) and X-ray diffraction from synchrotron radiation.[25] In addition, recently $BaBi_{0.5}{}^{3+}(Bi_{0.2}{}^{5+}Nb_{0.3}{}^{5+})O_3$ is reported to be ferroelectric at room temperature, although its average structure was described by a centrosymmetric space group $R\bar{3}$ with neutron diffraction data.[26] Therefore, careful structural studies on these systems are needed. Here the structural studies on the series $BaBi_{1-x}Ta_xO_3$ ($0 \le x \le 0.5$) are presented, which suggest that the whole series crystallizes in $P1$ at room temperature.

Experimental Section

The series $BaBi_{1-x}Ta_xO_3$ (x = 0, 0.025, 0.05, 0.075, 0.100, 0.125, 0.150, 0.175, 0.200, 0.225, 0.250, 0.275, 0.300, 0.350, 0.400, 0.450, and 0.500) has been synthesized from stoichiometric amounts of $BaCO_3$ (AR), Bi_2O_3 (AR), and Ta_2O_5 (99.95%). The oven-dried reagents were mixed and homogenized by grinding during about thirty minutes for a total of 6 g of mixtures with an agate mortar and a pestle. The mixtures were subjected to two 12 h calcinations at 750 °C with intermediate grindings. They were then pressed into pellets to undergo four 12 h heat treatments at 900 °C followed by a furnace cooling every time with intermediate grinding and then pressing into pellets. All the treatments were done in air. The weights of the samples were monitored before and after heat treatments. The maximum difference was about 4 mg for the 6 g samples. Therefore, the compositions of the samples were considered to be the same as the initial ones.

Powder X-ray diffraction (PXRD) data were collected on a Bruker D8 Advance diffractometer with Cu Kα1 (λ = 0.15407 nm) radiation (2θ range: 7−120°; step: 0.0197°; scan speed: 30 s/step) at 50 kV and 40 mA. Neutron powder diffraction (NPD) data were collected on an Echidna instrument at the OPAL reactor (Lucas Heights, Australia) with λ = 0.16215 and 0.24395 nm; samples were placed in 9 mm diameter vanadium cans and data collected over 4 h per sample. The X-ray and neutron diffraction data were analyzed using GSAS software.[27,28] Selected area electron diffraction (SAED) and convergent-beam electron diffraction (CBED) were carried out on a JEM2100F with an accelerating voltage of 200 kV. Capacitors for ferroelectric measurement were

(25) Hashimoto, T.; Tsuda, K.; Shiono, J.; Mizusaki, J.; Tanaka, M. *Phys. Rev. B* **2001**, *64*, 224114.
(26) Mangalam, R. V. K.; Mandal, P.; Suard, E.; Sundaresan, A. *Chem. Mater.* **2007**, *19*, 4114.
(27) Larson, A. C.; von Dreele, R. B. *Report LAUR 86-748*; Los Alamos National Laboratory, **1985**.
(28) Rietveld, H. M. *J. Appl. Crystallogr.* **1969**, *2*, 65.

Table 1. Rietveld Refinement Details of $BaBiO_3$ in Different Models

	model 1[b]	model 2	model 3
space group	*I*2/*m*	*P*1	*P*1[d]
lattice params	a = 0.6187(1) nm, b = 0.6141(1) nm, c = 0.8673(1) nm, β = 90.16(1)°	a = 0.6188(1) nm, b = 0.6142(1) nm, c = 0.8675(1) nm, α = 90.06(1)°, β = 90.16(1)°, γ = 90.00(1)°	a = 0. 6141(1) nm, b = 0.6186(1) nm, c = 0.6144(1) nm, α = 59.90(1)°, β = 59.98(1)°, γ = 59.87(1)°
atom	(x, y, z)	(x, y, z)	(x, y, z)
Ba1	0.5015 (1), 0.0000, 0.2495 (1)	0.5019 (1), −0.0092 (1), 0.2506 (1)	0.2513 (1), 0.2551 (1), 0.2438 (1)
Ba2		0.0008(1), 0.5064(1), 0.7485(1)	0.7454 (1), 0.7472 (1), 0.7577 (1)
Ba3		0.4998(1), −0.0049 (1), 0.7512 (1)	
Ba4		0.9989(1), 0.4856(1), 0.2549 (1)	
Bi1[a]	0.0000, 0.0000, 0.0000	0.0000, 0.0000, 0.0000	0.0000, 0.0000, 0.0000
Bi2	0.0000, 0.0000, 0.5000	0.4999(1), 0.5000(1), 0.5005(1)	0.5024(1), 0.5017(1), 0.5004(1)
Bi3		0.0017(1), −0.0035(1), 0.5010(1)	
Bi4		0.4994(1), 0.4954(1), 0.0013(1)	
O1	0.0619(1), 0.0000, 0.2604(1)	0.0710(1), −0.0075(1), 0.2626(1)	0.2268 (1), 0.2924 (1), 0.6990 (1)
O2	0.2625(1), 0.2421(1), 0.9667(1)	0.5496 (1), 0.4688(1), 0.7592(1)	0.7974 (1), 0.6922(1), 0.2834(1)
O3		0.9290(1), −0.0015(1), 0.7391(1)	0.7088 (1), 0.2760(1), 0.2349(1)
O4		0.4453(1), 0.4736(1), 0.2428 (1)	0.2511(1), 0.7018(1), 0.7924(1)
O5		0.2419(1), 0.2696(1), 0.9688(1)	0.2709(1), 0.8011(1), 0.2494(1)
O6		0.7513(1), 0.7658(1), 0.4667(1)	0.7266(1), 0.1978(1), 0.7545(1)
O7		0.7276(1), 0.2371(1), 0.0394(1)	
O8		0.2424(1), 0.7480(1), 0.5397(1)	
O9		0.7078(1), 0.7718(1), 0.0261(1)	
O10		0.2419(1), 0.2497(1), 0.5064(1)	
O11		0.2552(1), 0.7392(1), 0.9588(1)	
O12		0.7622(1), 0.2560(1), 0.4645(1)	
R factor[c]	R_{wp}^{x} = 0.070, R_{p}^{x} = 0.050 R_{wp}^{n1} = 0.075, R_{p}^{n1} = 0.058 R_{wp}^{n2} = 0.118, R_{p}^{n2} = 0.091	R_{wp}^{x} = 0.066, R_{p}^{x} = 0.047 R_{wp}^{n1} = 0.062, R_{p}^{n1} = 0.048 R_{wp}^{n2} = 0.123, R_{p}^{n2} = 0.095	R_{wp}^{x} = 0.063, R_{p}^{x} = 0.041 R_{wp}^{n1} = 0.069, R_{p}^{n1} = 0.052 R_{wp}^{n2} = 0.117, R_{p}^{n2} = 0.089

[a] In models 2 and 3, the site for Bi1 is set to (0.0000, 0.0000, 0.0000). [b] The atomic coordinates agree well with those reported in refs 7, 8. [c] R_{wp}^{x}, R_{p}^{x} are the R factors of the whole patterns and the peaks only for X-ray diffraction data, respectively; R_{wp}^{n1}, R_{p}^{n1} are the corresponding R factors for neutron diffraction data collected at the wavelength of 0.16215 nm; R_{wp}^{n2}, R_{p}^{n2} are the R factors for neutron diffraction data collected at the wavelength of 0.24395 nm. [d] The thermal displacing parameters for this phase, U_{equiv}, are listed below: Ba1, Ba2, 0.0090; Bi3, Bi4, 0.0071; O1, O2, O3, O4, O5, O6, 0.0172.

made by painting Ag paste on both sides of the pellet. The ferroelectric hysteresis was measured with a Radiant Technologies Inc. Precision Premier II. IR spectra were recorded on an ECTOR 22 FTIR spectrophotometer in the region of 650−50 cm^{-1} and on a Magna-IR 750 FTIR spectrophotometer in the region of 4000−400 cm^{-1}. Raman spectra were recorded on a Jobin-Yvon HR800 Raman spectrometer in the region of 2000−200 cm^{-1}.

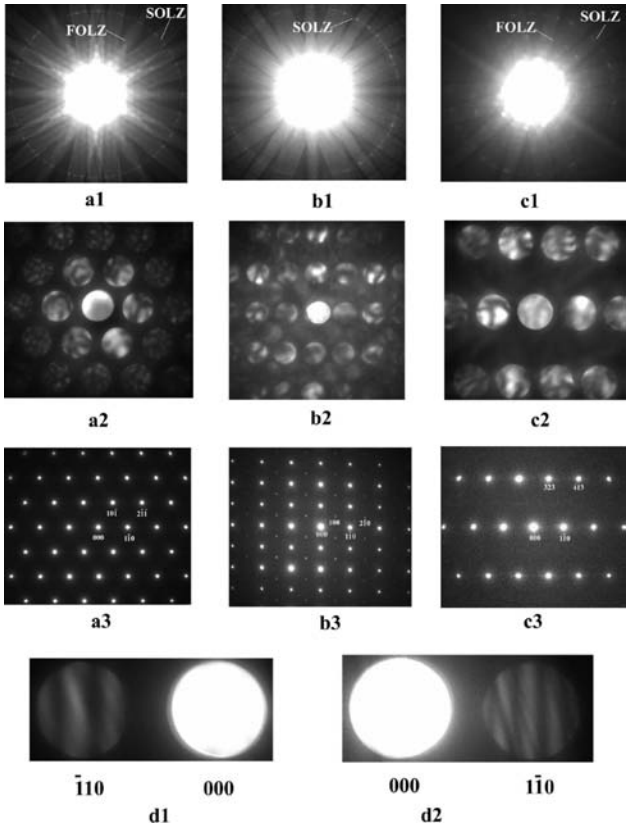

Figure 2. CBED pattern of $BaBiO_3$ (a1), the central part of a1 (a2), and the diffraction pattern of $BaBiO_3$ (a3) taken at [111] incidence; the CBED pattern (b1), the central part of b1 (b2), and the diffraction pattern (b3) taken at [001] incidence; the CBED pattern (c1), the central part of c1 (c2), and the diffraction pattern (c3) taken at [33$\bar{5}$] incidence; $\bar{1}10$ (d1) and $1\bar{1}0$ (d2) reflections of a dark field disk of $BaBiO_3$ taken at [111] incidence; the distributions of the intensities in the disks do not coincide with each other. Neither a rotation axis nor a mirror is observed from the CBED patterns.

Results and Discussions

Crystallographic Structure of $BaBiO_3$. At room temperature $BaBiO_3$ is reported to crystallize in *I*2/*m* with a = 0.6186 nm, b = 0.6140 nm, c = 0.8670 nm, β = 90.17° (model 1).[7−14] However, Hashimoto[25] has suggested that $BaBiO_3$ crystallizes in *P*1 with a = 0.6188 nm, b = 0.6139 nm, c = 0.8671 nm, α = 89.99°, β = 90.14°, γ = 90.02° (model 2). The powder X-ray and neutron diffraction data of $BaBiO_3$ can be fitted well with either model 1 or 2 using the Rietveld method. The refinement plots are shown in Figure 1, and the details are listed in Table 1. The atomic coordinates for model 1 agree well with those reported by Thornton et al.,[8] where according to the BVS calculation[29] the oxidation states of Bi1 and Bi2 are believed to be 3+ and 5+, respectively (the BVS for Bi1 and Bi2 is 3.77 and 5.45, respectively). The atomic coordinates used in model 2 are produced

(29) Brown, I. D.; Altermatt, D. *Acta Crystallogr. B* **1985**, *41*, 244−247.

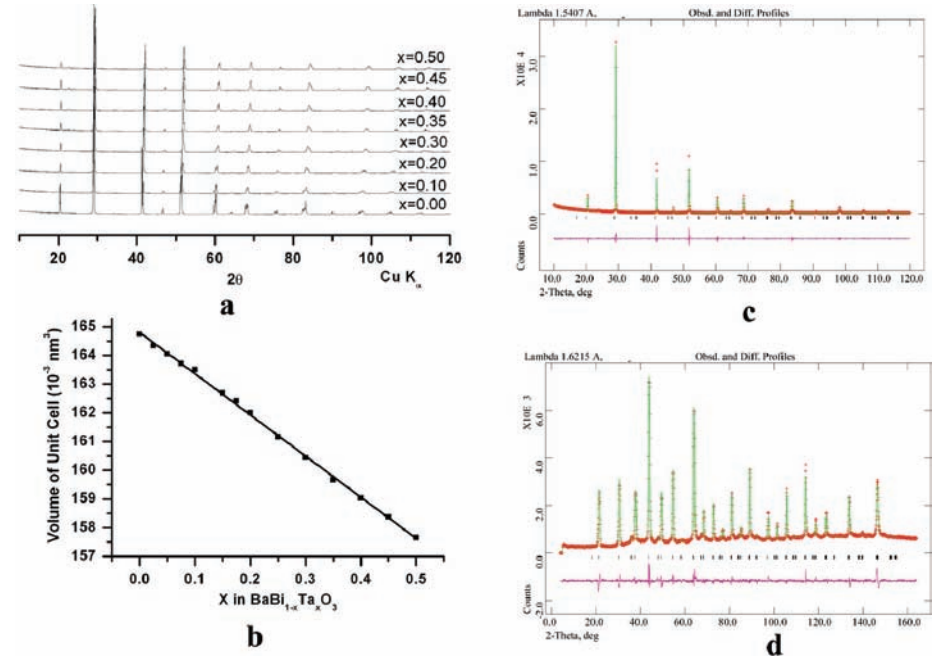

Figure 3. Powder X-ray diffraction patterns of the samples in the series $BaBi_{1-x}Ta_xO_3$ ($0 \le x \le 0.50$) (a); volume of the unit cell of the series $BaBi_{1-x}Ta_xO_3$ (b); the Rietveld plots of powder X-ray (c) and neutron (d) diffraction patterns for $BaBi_{1-x}Ta_xO_3$ ($x = 0.30$); the symbol + represents the observed value, the solid line represents the calculated value, the marks below the diffraction patterns are the calculated reflection positions, and the difference curve is shown at the bottom of the figure.

Table 2. Rietveld Refinement Details of $BaBi_{1-x}Ta_xO_3$ ($x = 0.30$)[a] in Space Group *P*1

atom	(x, y, z)	U_{equiv}	atom	(x, y, z)	U_{equiv}
Ba1	0.2523(1), 0.2515(1), 0.2465(1)	0.0236	O2	0.7187(1), 0.7714(1), 0.2749(1)	0.0625
Ba2	0.7420(1), 0.7470(1), 0.7692(1)	0.0236	O3	0.7375(1), 0.2554(1), 0.2538(1)	0.0625
Bi1[b]	0.0000, 0.0000, 0.0000	0.0197	O4	0.1758(1), 0.6980(1), 0.8171(1)	0.0625
Bi2/Ta	0.4994(1), 0.5008(1), 0.5021(1)	0.0197	O5	0.2631(1), 0.7933(1), 0.2335(1)	0.0625
O1	0.2224(1), 0.2809(1), 0.7404(1)	0.0625	O6	0.7535(1), 0.2739(1), 0.7394(1)	0.0625

[a] The lattice parameters are $a = 0.6102(1)$ nm, $b = 0.6106(1)$ nm, $c = 0.6097(1)$ nm, $\alpha = 59.99(1)°$, $\beta = 59.99(1)°$, $\gamma = 60.04(1)°$; the final refinement R factors are $R_{wp}{}^x = 0.114$, $R_p{}^x = 0.078$ for X-ray diffraction data and $R_{wp}{}^n = 0.063$, $R_p{}^n = 0.047$ for neutron diffraction data. [b] The site for Bi1 is set to (0.0000, 0.0000, 0.0000).

from those for model 1 with further refinements, where oxidation states of Bi1 and Bi2 are 3+, and the oxidation states of Bi3 and Bi4 are 5+ (see Supporting Information for details).

It is found that there are more peaks expected by model 2 than expected by model 1, and the intensity of most of these extra peaks is zero, which strongly implies that the lattice parameters of model 2 should be deduced or some symmetry operations are lost by model 2. However, Hashimoto[25] has strongly suggested that the symmetry of $BaBiO_3$ at room temperature is *P*1. Therefore, smaller lattice parameters are selected for $BaBiO_3$ as $a = 0.6141$ nm, $b = 0.6186$ nm, $c = 0.6144$ nm, $\alpha = 59.90°$, $\beta = 59.98°$, $\gamma = 59.87°$ (model 3) with the help of the software PowderCell.[30] The powder X-ray and neutron diffraction patterns can be fitted very well by this model (the details

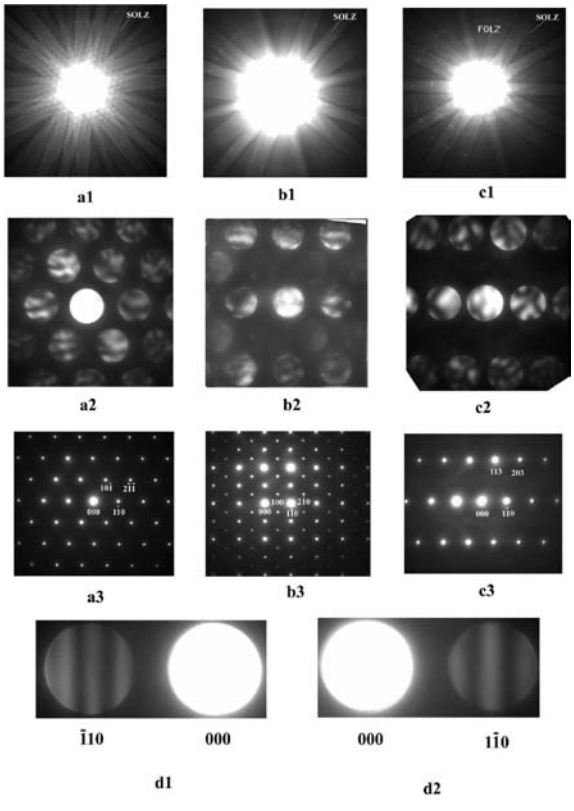

Figure 4. CBED pattern of $BaBi_{0.7}Ta_{0.3}O_3$ (a1), the central part of a1 (a2), and the diffraction pattern of $BaBi_{0.7}Ta_{0.3}O_3$ (a3) taken at [111] incidence; the CBED pattern (b1), the central part of b1 (b2), and the diffraction pattern (b3) taken at [001] incidence; the CBED pattern (c1), the central part of c1 (c2), and the diffraction pattern (c3) taken at [33$\bar{1}$] incidence; $\bar{1}10$ (d1) and $1\bar{1}0$ (d2) reflections of a dark field disk of $BaBiO_3$ taken at [111] incidence (d).

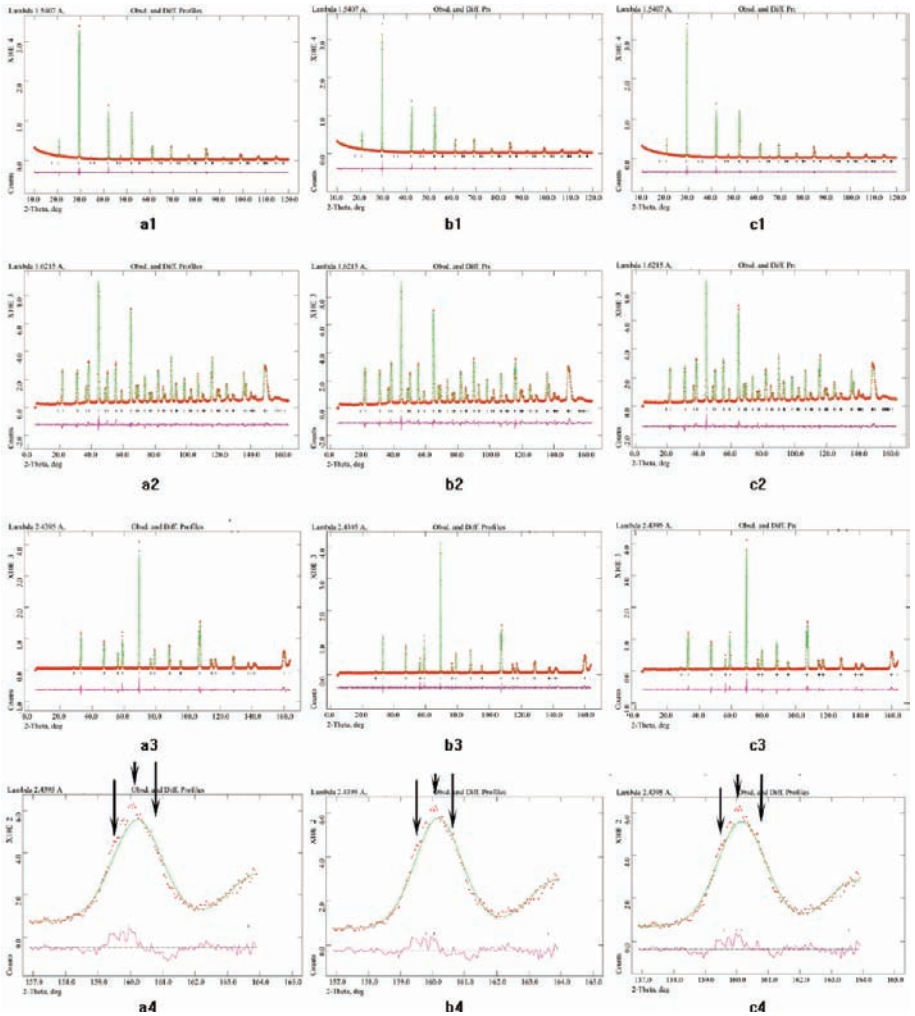

Figure 5. Rietveld plots of powder X-ray and neutron diffraction patterns for $BaBi_{0.5}Ta_{0.5}O_3$ using different space groups: model 4 (a1, X-ray (λ = 0.15407 nm); a2, neutron (λ = 0.16215 nm); a3, neutron (λ = 0.24395 nm); a4, part of a3), model 5 (b1, X-ray (λ = 0.15407 nm); b2, (λ = 0.16215 nm); b3, neutron (λ = 0.24395 nm); b4, part of b3), and model 6 (c1, X-ray (λ = 0.15407 nm); c2 (λ = 0.16215 nm); c3, neutron (λ = 0.24395 nm); c4, part of c3). The symbol + represents the observed value, the solid line represents the calculated value, the marks below the diffraction patterns are the calculated reflection positions, and the difference curve is shown at the bottom of the figure.

are listed in Table 1), as shown in Figure 1c. In this case, the number of expected peaks is a little more than that for model 1 and is much less than that for model 2. The difference between the expected diffraction peaks for model 1 and model 3 is too small to be detected when the wavelength is 0.15407 nm (for X-ray diffraction) or 0.16215 nm (for neutron diffraction), but a difference can be found at the 2θ range of 148° and 158° for the wavelength of 0.24395 nm, as shown in Figure 1 (a4 and c4; clearer figures are provided in the Supporting Information), where three peaks are expected by model 1 and four peaks are expected by model 3, with four observed peaks. Therefore, model 3 is better than model 1 to describe the structure of $BaBiO_3$ at room temperature.

Further, the selected area electron diffraction patterns of $BaBiO_3$ are checked to fit model 3 very well, as shown in Figure 2. The CBED patterns of $BaBiO_3$ are similar to those reported by Hashimoto et al.: neither a rotation axis nor a mirror is observed from the CBED patterns of $BaBiO_3$ taken at [111], [001], and [33$\bar{5}$] incidences; the distributions of the intensities in the disks of $\bar{1}10$ and $1\bar{1}0$ reflections do not coincide with each other, indicating that no inversion center exists.[25] Therefore, model 3 is believed to be a simple and correct description of the structure of $BaBiO_3$ at room temperature.

Crystallographic Structure of $BaBi_{1-x}Ta_xO_3$ ($0 < x < 0.5$). The powder X-ray diffraction patterns of the series $BaBi_{1-x}Ta_xO_3$ ($0 \le x \le 0.5$) are shown in Figure 3a for a direct view and are similar to each other. This implies that the structure of this series is the same. The structure of $BaBiO_3$ was used as the beginning model for the Rietveld refinement of the X-ray diffraction data of these samples. Acceptable fittings between the experimental data and the proposed models are obtained with $R_p < 7.9\%$, $R_{wp} < 11\%$ for all the data. As an example, the results of combined refinement of powder X-ray and neutron diffraction patterns for $BaBi_{1-x}Ta_xO_3$ (x = 0.30) are shown in Figure 3c,d. During the refinement, Ta atoms are restricted at the site for Bi^{5+} (see Supporting Information for further explanations). The occupation of Ta and Bi at

(30) Nolze, G.; Kraus, W. *Powder Diffr.* **1998**, *13*, 256.

Table 3. Rietveld Refinement Details of $BaBi_{0.5}Ta_{0.5}O_3$ in Different Models

	model 4[a]	model 5	model 6
space group	$R\bar{3}$	$I2/m$	$P1$[d]
lattice params	$a = b = c = 0.6048(1)$ nm, $\alpha = \beta = \gamma = 60.25(1)^o$	$a = 0.6050(1)$ nm, $b = 0.6070(1)$ nm, $c = 0.8573(1)$ nm, $\beta = 90.33(1)^o$	$a = 0.6049(1)$ nm, $b = 0.6073(1)$ nm, $c = 0.6071(1)$ nm, $\alpha = 60.05(1)^o$, $\beta = 59.90(1)^o$, $\gamma = 59.88(1)^o$
atom	(x, y, z)	(x, y, z)	(x, y, z)
Ba1	0.2506(1), 0.2506(1), 0.2506(1)	0.5066(1), 0.0000, 0.2480(1)	0.2462(1), 0.2510(1), 0.2478(1)
Ba2			0.7473(1), 0.7540(1), 0.7596(1)
Bi1[b]	0.0000, 0.0000, 0.0000	0.0000, 0.0000, 0.0000	0.0000, 0.0000, 0.0000
Ta1	0.5000, 0.5000, 0.5000	0.0000, 0.0000, 0.5000	0.5018(1), 0.4992(1), 0.5025(1)
O1	0.2261(1), 0.3114(1), 0.7319(1)	0.0360(1), 0.0000, 0.2606(1)	0.2270(1), 0.3198(1), 0.6764(1)
O2		0.2811(1), 0.2485(1), −0.0309(1)	0.7527(1), 0.7079(1), 0.2348(1)
O3			0.7377(1), 0.1973(1), 0.3256(1)
O4			0.2647 (1), 0.7910(1), 0.6936 (1)
O5			0.3003 (1), 0.7338(1), 0.2508(1)
O6			0.7300 (1), 0.2664(1), 0.7368(1)
R factor[c]	$R_{wp}^{x} = 0.060$, $R_p^{x} = 0.044$ $R_{wp}^{n1} = 0.060$, $R_p^{n1} = 0.046$ $R_{wp}^{n2} = 0.115$, $R_p^{n2} = 0.087$	$R_{wp}^{x} = 0.066$, $R_p^{x} = 0.048$ $R_{wp}^{n1} = 0.068$, $R_p^{n1} = 0.053$ $R_{wp}^{n2} = 0.123$, $R_p^{n2} = 0.091$	$R_{wp}^{x} = 0.059$, $R_p^{x} = 0.043$ $R_{wp}^{n1} = 0.061$, $R_p^{n1} = 0.048$ $R_{wp}^{n2} = 0.116$, $R_p^{n2} = 0.088$

[a] The atomic coordinates agree well with those reported in ref 16. [b] In model 6, the site for Bi1 is set to (0.0000, 0.0000, 0.0000). [c] R_{wp}^{x}, R_p^{x} are the R factors of the whole patterns and the peaks only for X-ray diffraction data, respectively; R_{wp}^{n1}, R_p^{n1} are the corresponding R factors for neutron diffraction data collected at the wavelength of 0.16215 nm; R_{wp}^{n2}, R_p^{n2} are the R factors for neutron diffraction data collected at the wavelength of 0.24395 nm. [d] The thermal displacing parameters for this phase, U_{equiv}, are listed below: Ba1, Ba2, 0.0089; Bi3, Bi4, 0.0093; O1, O2, O3, O4, O5, O6, 0.0239.

the Bi^{5+} site is set to $2x$:$2(0.5-x)$ without refinement. The details on the refinement of $BaBi_{0.7}Ta_{0.3}O_3$ as a typical example are listed in Table 2. Figure 3b shows the linear relation between the volume of the unit cell and the value of x in $BaBi_{1-x}Ta_xO_3$, which agrees well with Vigard's law.[31,32] In addition, the selected area electron diffraction (SAED) patterns of these samples are checked to fit the refinement model very well. The CBED patterns obtained for these samples confirm that they all crystallize in $P1$. As an example, Figure 4 shows the SAED and CBED patterns of $BaBi_{0.7}Ta_{0.3}O_3$: neither a rotation axis nor a mirror is observed from the CBED patterns of $BaBi_{0.7}Ta_{0.3}O_3$ taken at [111], [001], and [33$\bar{1}$] incidences; the distributions of the intensities in the disks of $\bar{1}10$ and $1\bar{1}0$ reflections do not coincide with each other, indicating that no inversion center exists.

Crystallographic Structure of $BaBi_{0.5}Ta_{0.5}O_3$. It has been reported that $BaBi_{0.5}Ta_{0.5}O_3$ is rhombohedral in $R\bar{3}$ with $a = 0.6048$ nm, $\alpha = 60.25°$ (model 4)[16] at room temperature. However, following the idea of the above section, $BaBi_{0.5}Ta_{0.5}O_3$ should crystallize in triclinic space group $P1$ with $a = 0.6049$ nm, $b = 0.6073$ nm, $c = 0.6071$ nm, $\alpha = 60.05°$, $\beta = 59.90°$, $\gamma = 59.88°$ (model 6). As shown in Figure 5, the X-ray and neutron diffraction data can be fitted well with these two models. The details of the above refinement are listed in Table 3. However, there are differences between these two models. For example, there are three peaks observed between 157° and 162° for the neutron diffraction data collected at a wavelength of 0.24395 nm (Figure 5), only one peak is expected by model 4 ($R\bar{3}$), and three peaks are expected by model 6 ($P1$). Therefore, we suggest that $BaBi_{0.5}Ta_{0.5}O_3$ crystallizes in $P1$. Several other models have also been checked. For example, the details of a monoclinic model (model 5 with the space group $I2/m$) are listed in Table 3 and shown in Figure 5. Only two peaks are expected between 157° and 162° for the neutron diffraction data collected at a wavelength of 0.24395 nm by this model, which indicates that this model is worse than model 6 (see Supporting Information for details). Therefore, it is reasonable to suggest that $BaBi_{0.5}Ta_{0.5}O_3$ crystallizes in space group $P1$ at room temperature.

The selected area electron diffraction patterns of $BaBi_{0.5}Ta_{0.5}O_3$ are checked to fit model 6 well as shown in Figure 6. The CBED patterns of $BaBi_{0.5}Ta_{0.5}O_3$ obtained are similar to that of $BaBiO_3$: neither a rotation axis nor a mirror is observed from the CBED patterns of $BaBiO_3$ taken at [111], [001], and [11$\bar{5}$] incidences; the distributions of the intensities in the disks of $\bar{1}10$ and $1\bar{1}0$ reflections do not coincide with each other, indicating that no inversion center exists. These confirm that the symmetry of $BaBi_{0.5}Ta_{0.5}O_3$ is $P1$.

Raman and FTIR Spectra. Raman and FTIR spectra have been used by Sugai[24] to suggest that an inversion center is absent in the crystal structure of $BaBiO_3$. In

(31) Vegard, L. *Z. Phys.* **1921**, *5*, 17.
(32) Vegard, L. *Z. Kristallogr.* **1928**, *67*, 239.

order to confirm our suggestion that no inversion center is in the crystal structure of $BaBi_{0.5}Ta_{0.5}O_3$ (we have suggested that $BaBi_{0.5}Ta_{0.5}O_3$ crystallizes in $P1$), Raman and FTIR spectra are collected for $BaBiO_3$ (for comparison) and $BaBi_{0.5}Ta_{0.5}O_3$, which are shown in Figure 7. The Raman data obtained for $BaBiO_3$ at room temperature are similar to those reported by Sugai,[24,33] and the IR data are similar to those reported by Uchida.[34] The partial overlaps of the Raman peaks and IR peaks for $BaBiO_3$ indicate that there is no inversion symmetry for $BaBiO_3$.[24] Therefore, the partial overlaps of the Raman peaks and IR peaks found for $BaBi_{0.5}Ta_{0.5}O_3$ also indicate that $BaBi_{0.5}Ta_{0.5}O_3$ has no inversion symmetry, which agrees well with our suggestion that $BaBi_{0.5}Ta_{0.5}O_3$ crystallizes in $P1$ instead of $R\bar{3}$.

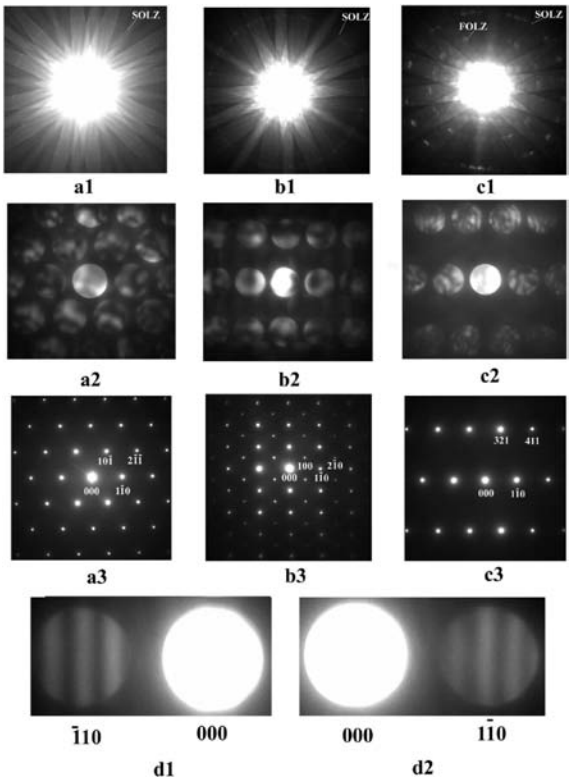

Figure 6. CBED pattern of $BaBi_{0.5}Ta_{0.5}O_3$ (a1), the central part of a1 (a2), and the diffraction pattern of $BaBi_{0.5}Ta_{0.5}O_3$ (a3) taken at [111] incidence; the CBED pattern (b1), the central part of b1 (b2), and the diffraction pattern (b3) taken at [001] incidence; the CBED pattern (c1), the central part of c1 (c2), and the diffraction pattern (c3) taken at [11$\bar{5}$] incidence; $\bar{1}10$ and $1\bar{1}0$ reflections of a dark field disk of $BaBi_{0.5}Ta_{0.5}O_3$ taken at [111] incidence (d).

Hysteresis Loop and Conductivity. As mentioned above, the series $BaBi_{1-x}Ta_xO_3$ crystallize in triclinic space group $P1$, which permits this series to be potential ferroelectrics.[35] Therefore, hysteresis loops of the series $BaBi_{1-x}Ta_xO_3$ were measured using a Radiant Technologies Inc. Precision Premier II. As it is known, Precision Premier II measures the quantity of electrical charge as the polarization of the tested sample, which always has the contribution from the capacitor and the resistor effects of the tested sample:

$$\begin{aligned} dQ_T &= c\,dV + I\,dt + dQ_F \\ &= c\,dV + V/R\,dt + dQ_F \end{aligned} \quad (1)$$

where Q_T is the total quantity of electrical charge measured by Precision Premier II, c is the capacitor, V is the driving voltage, I is the current caused by the resistor ($I = V/R$), R is the resistor of the sample, t is the charging time, and Q_F is the quantity of electrical charge caused by ferroelectric polarization. During the measurement, the driving voltage is changed linearly. Therefore,

$$V = \begin{cases} At & (-V_{max} \rightarrow V_{max}) \\ -At & (V_{max} \rightarrow -V_{max}) \end{cases} \quad (2)$$

$$\frac{1}{A} = \left|\frac{dt}{dV}\right| \approx \frac{\Delta t}{|\Delta V|} \quad (3)$$

where A is the speed of the change of voltage and V_{max} is the maximum of the driving voltage. During the measurement, $|\Delta V|$ changes with the driving voltage, and Δt is chosen as willing. If c, R, and A are not supposed to change with voltage, then

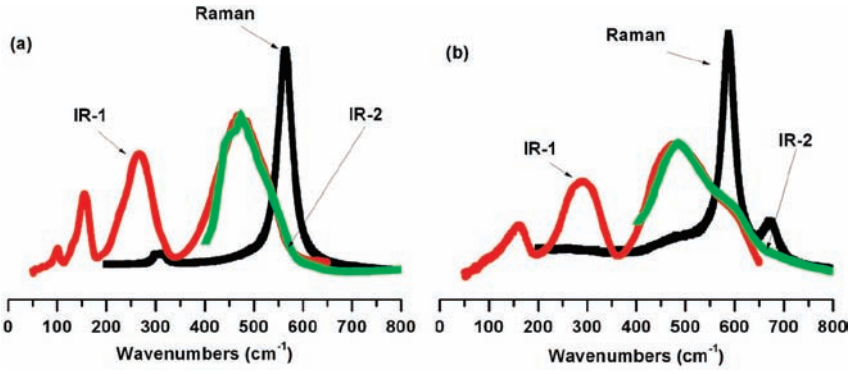

Figure 7. Raman and IR spectra of $BaBiO_3$ (a) and $BaBi_{0.5}Ta_{0.5}O_3$ (b). Raman are Raman spectra recorded on a Jobin-Yvon HR800 Raman spectrometer (France); IR-1 are FTIR spectra recorded on an ECTOR 22 FTIR spectrophotometer in the region 650−50 cm^{-1}; IR-2 are data recorded on a Magna-IR 750 FTIR spectrophotometer.

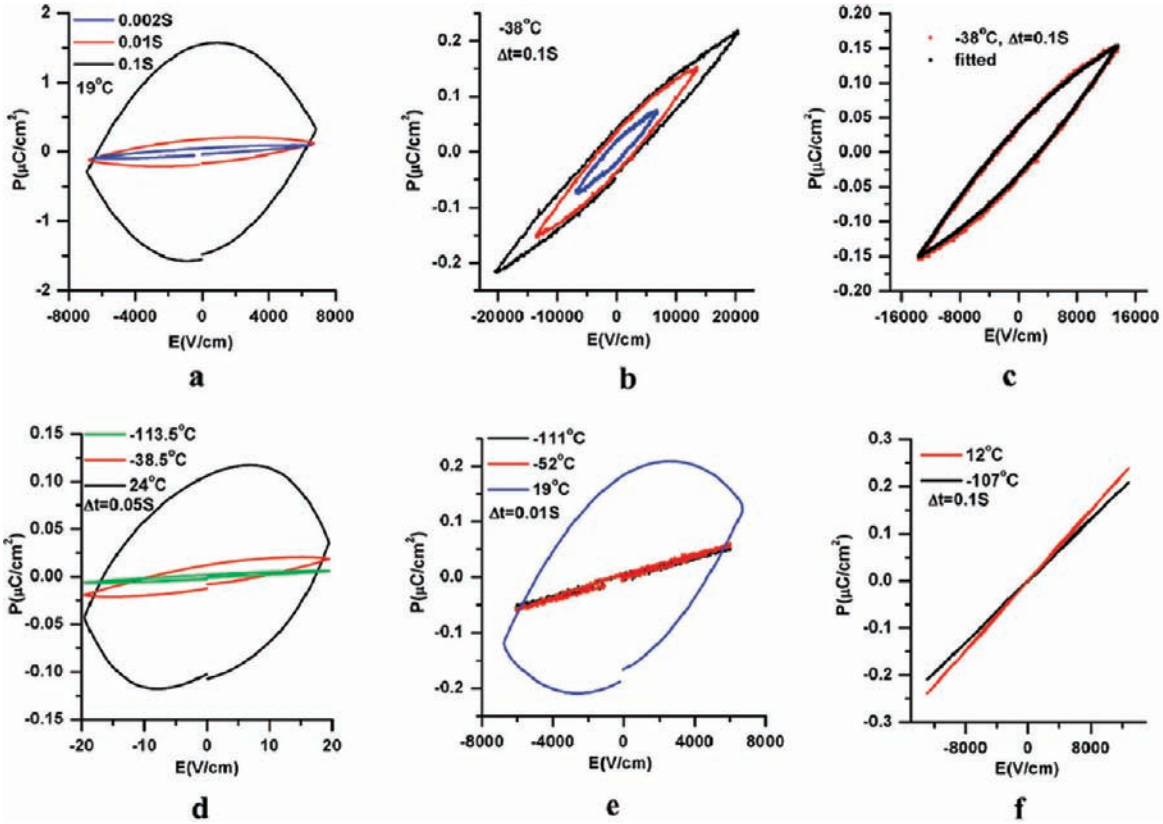

Figure 8. Hysteresis loops measured at 19 °C for $BaBi_{0.7}Ta_{0.3}O_3$ at various charging time (a); measured at −38 °C for $BaBi_{0.7}Ta_{0.3}O_3$ at various driving voltages (b); measured and fitted data for $BaBi_{0.7}Ta_{0.3}O_3$ (c); measured at various temperatures for $BaBiO_3$ (d); measured at various temperatures for $BaBi_{0.7}Ta_{0.3}O_3$ (e); measured at various temperatures for $BaBi_{0.5}Ta_{0.5}O_3$ (f).

$$Q_T = \begin{cases} cV + \dfrac{V^2}{2RA} + Q_F \approx cV + \dfrac{V^2}{2R}\dfrac{\Delta t}{|\Delta V|} + Q_F & (-V_{max} \rightarrow V_{max}) \\ cV + \dfrac{V_{max}^2}{RA} - \dfrac{V^2}{2RA} + Q_F \approx cV + \left(\dfrac{V_{max}^2}{R} - \dfrac{V^2}{2R}\right)\dfrac{\Delta t}{|\Delta V|} + Q_F & (V_{max} \rightarrow -V_{max}) \end{cases} \quad (4)$$

Typical hysteresis loops for the series $BaBi_{1-x}Ta_xO_3$ are shown in Figure 8. Figure 8a shows the hysteresis loops for $BaBi_{0.7}Ta_{0.3}O_3$ measured at 19 °C at different Δt. With the increase of Δt, the measured loop becomes larger, indicating that the contribution from the resistor effect of the sample is very significant. Figure 8b shows the hysteresis loops of $BaBi_{0.7}Ta_{0.3}O_3$ measured at 19 °C at various driving voltages; their shapes are similar. All of them can be fitted by eq 4 very well with $Q_F \approx 0$ as shown in Figure 8c. This indicates that the present data do not suggest that $BaBi_{0.7}Ta_{0.3}O_3$ is ferroelectrics. Similar results are obtained for the other samples in the series $BaBi_{1-x}Ta_xO_3$. Therefore, it is reasonable to suggest that the series $BaBi_{1-x}Ta_xO_3$ is not ferroelectric (or, it is better to say that the ferroelectric effect of the series $BaBi_{1-x}Ta_xO_3$ is too weak to be observed from the ceramic samples).

Typical data for $BaBiO_3$, $BaBi_{0.7}Ta_{0.3}O_3$, and $BaBi_{0.5}Ta_{0.5}O_3$ down to about −110 °C are shown in Figure 8d,e, f, respectively. It is found that with the decrease in temperature, the contribution from the resistor effect becomes weak because of the increase of the resistor of the sample, as indicated by the temperature-dependent conductivity data shown in Figure 9. Because of the low conductivity, the hysteresis loop of $BaBi_{0.5}Ta_{0.5}O_3$ at 12 °C is linear, which is mainly contributed by the capacitor effect of the sample.

The conductivity data of the series $BaBi_{1-x}Ta_xO_3$ were obtained by measuring the leakage current of the corresponding sample using a Radiant Technologies Inc. Precision Premier II. The corresponding data of $BaBiO_3$, $BaBi_{0.7}Ta_{0.3}O_3$, and $BaBi_{0.5}Ta_{0.5}O_3$ are shown in Figure 9. The conductivity of $BaBiO_3$ decreases with a decrease in temperature, which is very similar to the reported data.[36,37] The conductivity of $BaBiO_3$ is high, so the driving voltage must be low to make sure that the

(33) Sugai, S.; Uchida, S.; Kitazawa, K.; Tanaka, S.; Katsui, A. *Phys. Rev. Lett.* **1985**, *55*, 426–429.
(34) Uchida, S.; Tajima, S.; Masaki, A.; Sugai, S.; Kitazawa, K.; Tanaka, S. *J. Phys. Soc. Jpn.* **1985**, *54*, 4395–4409.
(35) Blinc, R.; Zeks, B. *Soft Modes in Ferroelectrics and Antiferroelectrics*; North-Holland: Amsterdam, 1974.
(36) Iguchi, E.; Nakamura, N.; Aoki, A. *J. Phys. Chem. Solids* **1997**, *58*, 755.
(37) Ghosh, A. *Solid State Commun.* **1999**, *112*, 45.

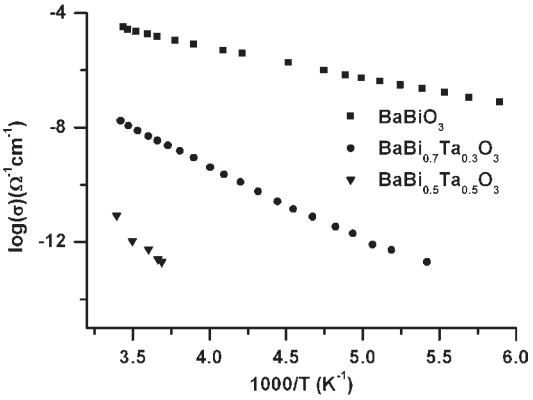

Figure 9. Temperature-dependent conductivities of $BaBiO_3$, $BaBi_{0.7}Ta_{0.3}O_3$, and $BaBi_{0.5}Ta_{0.5}O_3$.

measured signal is lower than the upper limit of the Precision Premier II.

When more Bi is changed to Ta in the series $BaBi_{1-x}Ta_xO_3$, the conductivity of the sample decreases. Therefore a high driving voltage can be used for $BaBi_{0.7}Ta_{0.3}O_3$ and $BaBi_{0.5}Ta_{0.5}O_3$. The conductivity data of $BaBi_{0.5}Ta_{0.5}O_3$ below −20 °C are not obtained because the measured signal is around the lower limit of the Precision Premier II.

Conclusion

The series $BaBi_{1-x}Ta_xO_3$ ($0 \leq x \leq 0.5$) has been synthesized by solid-state reactions under 900 °C. By the combined use of the CBED and the powder X-ray and neutron diffraction, their space group is determined to be *P*1. However, the current hysteresis measurement does not show that they are ferroelectrics.

Acknowledgment. This work is supported by the National Natural Science Foundation of China (Grants 20771008) and partially supported by a National Key Basic Research Project of China (2010CB833103). We thank Dr. M. Avdeev for assistance collecting the neutron power diffraction data at the OPAL facility.

Supporting Information Available: Oxidation states of Bi's in the different models of $BaBiO_3$ and the Rietveld plots of powder X-ray and neutron diffraction patterns for $BaBiO_3$ and $BaBi_{0.5}Ta_{0.5}O_3$. This material is available free of charge via the Internet at http://pubs.acs.org.